JCTC Journal of Chemical Theory and Computation

Comparative Study on the Performance of Hybrid DFT Functionals in Highly Correlated Oxides: The Case of CeO_2 and Ce_2O_3

Jesús Graciani,[†] Antonio M. Márquez,[†] José J. Plata,[†] Yanaris Ortega,[†] Norge C. Hernández,[‡] Alessio Meyer,[§] Claudio M. Zicovich-Wilson,[||] and Javier Fdez. Sanz*,[†]

Departamento de Química Física, Facultad de Química, Universidad de Sevilla, 41012 Sevilla, Spain; Departamento de Física Aplicada I, Universidad de Sevilla, 41011 Sevilla, Spain; Dipartimento IFM, Università di Torino, Via P. Giuria, 7, I-10125 Torino, Italy and Unitá INFM di Torino, Sezione F, via Giuria 5, I-10125 Torino, Italy; and Facultad de Ciencias, Universidad Autonoma del Estado de Morelos, Av. Universidad 1001, 62209 Cuernavaca, México

Received August 3, 2010

Abstract: The outstanding catalytic properties of cerium oxides rely on the easy $Ce^{3+} \leftrightarrow Ce^{4+}$ redox conversion, which however constitutes a challenge in density functional based theoretical chemistry due to the strongly correlated nature of the 4*f* electrons present in the reduced materials. In this work, we report an analysis of the performance of five exchange-correlation functionals (HH, HHLYP, PBE0, B3LYP, and B1-WC) implemented in the CRYSTAL06 code to describe three properties of ceria: crystal structure, band gaps, and reaction energies of the $CeO_2 \rightarrow Ce_2O_3$ process. All five functionals give values for cell parameters that are in fairly good agreement with experiment, although the PBE0 hybrid functional is found to be the most accurate. Band gaps, 2*p*-4*f*-5*d* in the case of CeO_2 and 4*f*-5*d* in the case of Ce_2O_3, are found to be, in general, overestimated and drop off when the amount of Hartree−Fock exchange in the exchange-correlation functional decreases. In contrast, the reaction energies are found to be underestimated, and increase when the amount of HF exchange lowers. Overall, at its standard formulation, the B1-WC functional seems to be the best choice as it provides good band gaps and reaction energies, and very reasonable crystal parameters.

1. Introduction

Cerium oxides, either CeO_2 or nonstoichiometric CeO_{2-x}, hereafter referred to generically as ceria, have traditionally played the role of a support material in components of catalysts used in several chemical processes. Typical examples of industrial applications are the three-way catalysts in automotive catalytic converters, fluid-cracking catalysts in refineries, and ethylbenzene dehydrogenation catalysts used during the production of styrene.[1,2] Ceria is also an active component in low-temperature CO and VOC oxidation catalysts, wet-oxidation of organic pollutants in water, hydrocarbon-reforming and the water-gas-shift reaction. Initially, the promoting effect of ceria was attributed to the enhancement of the metal dispersion and the stabilization toward thermal sintering.[3,4] However, subsequent work has shown that ceria can act as a chemically active component as well, working as an oxygen reservoir able to deliver it in the presence of reductive gases and to incorporate it upon interaction with oxidizing gases.[5−7] Its ability to store, release, and transport oxygen ions indicates

* Corresponding author e-mail: sanz@us.es.

[†] Departamento de Química Física, Facultad de Química, Universidad de Sevilla.

[‡] Departamento de Física Aplicada I, Universidad de Sevilla.

[§] Dipartimento IFM, Università di Torino and Unitá INFM di Torino.

[||] Facultad de Ciencias, Universidad Autonoma del Estado de Morelos.

10.1021/ct100430q
Published on Web 12/01/2010

that ceria is not just a mere spectator but it takes part in the catalytic reaction. For instance, in the case of oxidation reactions catalyzed by vanadia, the catalytic activity appears to be highly enhanced when supported on ceria as compared to more inert supports as silica and alumina.[8−11] Similar behavior is clearly seen in the case of the water−gas shift reaction, where experiments carried on Rh/CeO_2 and on pure CeO_2[12,13] reveal striking differences. Also, the very recent work of Park et al.[14] and of Rodriguez et al.[15,16] illustrates the importance of stabilizing Ce^{3+} centers and the role of the ceria nanoparticles.

The outstanding properties of ceria, and, consequently, the broad use in heterogeneous catalysis are due to its facile $Ce^{3+} \leftrightarrow Ce^{4+}$ redox conversion,[17] however, the adequate description of the electronic configuration of Ce^{3+} ions constitutes a challenge in density functional based theoretical chemistry due to the strongly correlated nature of the 4*f* electrons. Indeed, the 4*f* electrons in Ce_2O_3 are localized and the material behaves like a typical antiferromagnetic Mott−Hubbard insulator.[18] However, due to the well-known lack of cancellation of the Coulomb self-interaction, DFT approaches within the LDA or GGA frameworks predict metallic behavior.[19−26] To circumvent this problem within the DFT framework, the use of hybrid functionals, in particular the Heyd−Scuseria−Ernzerhof (HSE06) hybrid[27] has been recently reported for both fully reduced bulk Ce_2O_3,[23,28] and partially reduced CeO_2 (111) surfaces.[29] Alternatively, a much less demanding computational approach makes use of a Hubbard-like term to account for the strong *on-site* Coulomb interactions. Indeed, the choice of *U* is a delicate point as the physical idea behind the method is to improve the electron correlation description of an electron pair in a given orbital, and it is clear that the optimum *U* value for LDA and GGA can be different. Also, the *U* parameter has to be large enough to properly localize the 4*f* electron of Ce^{3+}, but without introducing undesired artifacts, such as overestimated band-gaps, and finally, as recently suggested by Castleton et al.,[25] the *U* value might be different for different properties under study. This latter aspect is not of minor importance as, for instance, the *U* value that better gives the lattice parameters must not necessarily provide the best energies or band gaps. Finally, one has to mention the possibility of using a *U* value determined in a self-consistent way: $U_{eff} = 5.30$ and 4.50 eV for LDA and GGA, respectively.[30,31] However, there is no guarantee that a self-consistent *U* will systematically improve calculated results. In this context, it is also worth mentioning that a recent work on lanthanide oxides using a many-body perturbation theory in the *GW*@LDA+*U* approach exhibits only a weak dependence on *U* in a physically meaningful range of *U* values.[32]

In spite of the empirical choice of the *U* parameter,[21,22] the DFT+*U* approach has been shown to be an effective, widely used, theoretical tool in the study of structure and reactivity of ceria surfaces. However, for accurate energies and properties, an approach without external semiempirical input appears to be preferable. For instance, let us consider the case of CeO_2 fluorite structure for which the experimental value is $a_0 \approx 5.41$ Å (5.406 Å[33] or 5.411 Å[34]). The LDA+U ($U_{eff} = 5.30$ eV) value is $a_0 = 5.40$ Å, in good agreement with the experiment, while GGA (PBE+U, $U_{eff} = 4.5$ eV)[23] moderately overestimates it: $a_0 = 5.49$ Å. This 1.3% error of the GGA represents a 4.5% increase in the equilibrium volume and it has been shown to be critical in the determination of the charge state of gold atoms deposited on CeO_2 (111) surfaces.[35−37] In its turn, a very accurate a_0 value results from hybrid DFT calculations: 5.39 and 5.40 Å from plane-wave calculations with the PBE0 and HSE hybrid functionals, respectively,[23] or 5.41 Å from calculations using a Gaussian-Type Orbitals (GTO) basis set and the HSE functional.[28]

The performance of both the DFT+*U* and the hybrid DFT approaches to describe the electronic properties of ceria has been analyzed in a series of papers. For instance, Hay et al.[28] compared the suitability of LDA, GGA and meta-GGA DFT functionals with HSE06 hybrid calculations using a GTO basis set. Furthermore, Da Silva et al.[23] compared PBE0 and HSE functionals using a plane wave basis set, and more recently, Kullgren et al.[38] have reported on the performance of B3LYP calculations. In the latter work, it was shown for instance that B3LYP performs slightly better than PBE0 for the electronic properties but slightly worse for the structural properties.

The work reported so far on the performance of the DFT functionals to describe the electronic properties of ceria makes it clear that hybrid functionals are better suited than DFT+*U* techniques to correctly render the structural and electronic properties of reduced ceria-based systems. Unfortunately, periodic hybrid DFT calculations face a number of computational problems that make them computationally demanding. Briefly, if we consider the plane-wave and GTO implementations, we find that energy calculations are reasonably fast when using GTO but geometry optimization becomes slow because the calculation of energy gradients in a GTO basis set becomes, generally speaking, the limiting step regardless the functional used. The choice of the basis set is also a key question especially for the 4*f* shell. In contrast, geometry optimizations are in general much more efficient when using a plane-wave basis set, but here the limiting step is the calculation of the energy with the hybrid functional due to the difficulty to estimate the nonlocal Fock exchange contribution. Finally, one must realize that hybrid DFT is sensitive to an additional factor because the amount of Fock exchange included in the potential is also an external input which largely affects the final description.[39,40]

Despite the recent efforts devoted to elucidate the properties of reduced ceria samples, and the ability of hybrid functionals to describe them, the body of literature about the subject still is scarce. In particular, most of the work has mainly been focused on structural and electronic aspects, while the energetic aspects, which are of major interest in chemistry, had not been in general considered. Moreover, a complete analysis of the dependence of the 4*f* band splitting, as well as the different band-gaps, cell parameters, and heats of formation on the amount of the exact exchange has not been yet reported. Indeed, as reported by Moreira et al. in their work on NiO,[40] the fraction of Fock exchange introduced in the hybrid functional does alter not only the

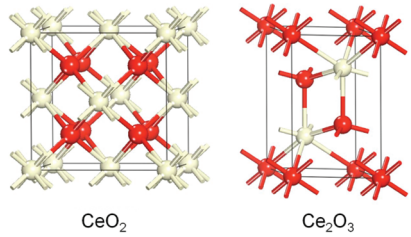

Figure 1. Left: Fluorite type structure of CeO_2 (face-centered cubic, $Fm\bar{3}m$). Right: the sesquioxide A-type structure of Ce_2O_3 (hexagonal, $P\bar{3}m1$). Red and white balls indicate O and Ce atoms, respectively.

band-gaps but also the lattice constant, and the elastic constants and bulk modulus.

In view of the importance of this class of material, and the lack of information about the suitability of hybrid functionals to render a specific property, we have carried out in the present work a systematic analysis of the performance of five functionals commonly used in the literature, and that are implemented in the CRYSTAL06 code, namely the Perdew−Burke−Ernzerhof PBE0, the half and half HH, the modified half and half HHLYP, the widely used in computational chemistry B3LYP, and the recently proposed B1-WC functional. Using a purely ab initio periodic framework and treating oxidized and reduced ceria on an equal footing, we focus on the response of these functionals on three different sets of data: (i) structure: lattice parameters for CeO_2 and Ce_2O_3; (ii) band gaps: $2p$-$4f$-$5d$ in the case of CeO_2 and $4f$-$5d$ in the case of Ce_2O_3; and (iii) reaction energies involved in the CeO_2/Ce_2O_3 redox process. Moreover, bearing in mind the aforementioned sensitivity of the hybrid functionals to the fraction of exchange included, a systematic analysis of the behavior of the PBE0, B3LYP, and B1-WC functionals that incorporate different amounts of exact Fock exchange is also reported.

2. Computational Details

Two different structures were studied in this work, the CeO_2 fluorite crystal ($Fm\bar{3}m$) and the Ce_2O_3 A-type crystal ($P\bar{3}m1$). Their unit cells are shown in Figure 1. All of the calculations were performed using a developing version of the CRYSTAL06 code,[41] where the Fock (and Kohn−Sham, KS) equations[42] for the valence electron density are solved in a periodic framework. In this framework, the crystalline orbitals are represented as linear combinations of Bloch functions (BFs) and are evaluated over a regular three-dimensional mesh in the reciprocal space. Each BF is built from atom-centered atomic orbitals (AOs) that are contractions (linear combinations with constant coefficients) of Gaussian-type functions (GTFs), each GTF being the product of a Gaussian times a real solid spherical harmonic.

Five hybrid DFT functionals were used in this work: PBE0,[43] HH, HHLYP,[44] B3LYP,[45−47] and the recently proposed B1-WC functional.[48] Self-consistent-field (SCF) closed shell calculations were performed to obtain the ground electronic state in the case of CeO_2, while in the case of Ce_2O_3 spin-polarized calculations were performed in order to discriminate between the ferromagnetic and antiferromagnetic states of this oxide. In the latter, multiple solutions of the SCF take place depending on the accommodation of the unpaired electrons over the Ce $4f$ AOs. A recent implementation in the CRYSTAL program allows us to favor the convergence into a given symmetry adapted electronic configuration through a proper definition of the initial guess. In Ce_2O_3 calculations, the most stable configuration for the $4f$ electrons in Ce has been chosen. This is an antiferromagnetic state where both α and β electrons occupy a mixing between $(2z^2 - 3x^2 - 3y^2)z$ and $(x^2 - 3y^2)x$ components of the $4f$ AOs of Ce.

The PBE0 is a combination of the GGA exchange-correlation functional PBE[49] (E_{XC}^{PBE}) and the exact Hartree−Fock (HF, E_X^{HF}) exchange following the expression:

$$E_{XC}^{PBE0} = E_{XC}^{PBE} + 1/4(E_X^{HF} - E_X^{PBE}) \quad (1)$$

The HH, HHLYP, B3LYP, and B1-WC follow the expression:

$$E_{XC} = (1\text{-A})(E_X^{LDA} + BE_X^{BECKE/WC}) + AE_X^{HF} + (1\text{-C})E_C^{VWN} + CE_C^{LYP/PBE} \quad (2)$$

where E_X^{LDA} is the exchange contribution by using the Dirac−Slater functional[50] and E_C^{VWN} is the correlation energy coming from the use of the Volsko−Wilk−Nusair parametrization of the Ceperley−Alder free electron gas correlation results.[51] In the case of HH, HHLYP, and B3LYP functional, $E_X^{BECKE/WC}$ stands for the Becke's exchange,[52] and $E_C^{LYP/PBE}$ represents the Lee−Yang−Parr correlation energy.[46] In the case of the B1-WC functional, $E_X^{BECKE/WC}$ stands for the Wu−Cohen[53] GGA exchange, and $E_C^{LYP/PBE}$ is the correlation energy contribution from the PBE.[49] Concerning the three weight parameters, $A = 0.2$, $B = 0.9$, and $C = 0.81$ for B3LYP. These parameters are set to $A = 0.5$ and $C = 1.0$ when we deal with the HH ($B = 0.0$) and HHLYP ($B = 1.0$) functional. In the case of using the B1-WC functional, $A = 0.16$ and $B = C = 1.0$.

Although calculations using the HSE06 functional are not performed in this work, we will also briefly outline it since is closely related to the PBE0 and largely used in the comparisons reported here. In the HSE functional, the spatial decay of the HF exchange interaction is accelerated by partitioning the Coulomb potential for exchange into short-range (SR) and long-range (LR) components:[27]

$$E_{XC}^{HSE} = aE_X^{HF,SR}(\omega) + (1\text{-a})E_X^{PBE,SR}(\omega) + E_X^{PBE,LR}(\omega) + E_C^{PBE} \quad (3)$$

where the mixing coefficient a is set to 0.25, and the screening factor ω defines the separation range. This enables a substantial lowering of the computational cost for calculations in extended systems. Note that in the limit $\omega = 0$, HSE reduces to the hybrid functional PBE0, and when $\omega \rightarrow \infty$, *HSE becomes identical with PBE.*

Inner electrons of Ce atom were replaced by an effective core potential developed by the Stuttgart−Dresden group.[54] The Ce electrons explicitly treated were the $4s^2 4p^6 4d^{10} 5s^2 5p^6 4f^1 6s^2 5d^1$, with a (10sp7d8f)/[4sp2d3f] basis

Table 1. Calculated and Experimental Lattice Parameters (in Å) for CeO_2 and Ce_2O_3

	CeO_2		Ce_2O_3				
method	a_0	error	a_0	error	c_0	error	refs
B3LYP	5.47	0.06	3.89	0.00	6.17	0.11	
HH	5.34	−0.07	3.83	−0.06	5.93	−0.13	
HHLYP	5.42	0.01	3.88	−0.01	6.14	0.08	
PBE0	5.40	−0.01	3.86	−0.03	6.04	−0.02	
B1-WC	5.38	−0.03	3.84	−0.05	5.93	−0.13	
GGA(PBE)+U($U = 4.5$)			3.87	−0.02	5.93	−0.13	24
GGA(PW91)+U($U = 3.0$)	5.48	0.07	3.92	0.03			22
HSE	5.41	0.00	3.87	−0.02	6.06	0.00	23
PBE0	5.39	−0.02	3.87	−0.02	6.07	0.01	23
Experiment	5.41		3.89		6.06		33,34

set optimized to properly describe oxides where the metal features III and IV oxidation states. The corresponding exponents and coefficients can be found in ref 55. For O an all-electron basis set proposed in ref 56 for ionic crystals was adopted. The two most external *sp* and *d* exponents have been reoptimized for cerium oxide, their resulting values being 0.4798717, 0.1801227, and 0.2991812 $bohr^{-2}$, respectively.

Other technical parameters were set as follow. With the aim of obtaining an enough level of accuracy when evaluating the Coulomb and exchange series the five thresholds had the values of 10^{-8}, 10^{-8}, 10^{-8}, 10^{-8}, and 10^{-20}. The Brillouin zone was sampled using a $6 \times 6 \times 6$ Monkhorst-Pack[57] grid, corresponding to 16 reciprocal space irreducible points at which the KS matrix was diagonalized. The SCF calculations were considered to be converged when the energy changes between the iterations were smaller than 10^{-8} hartree. The exchange-correlation contribution to the energy was evaluated by numerical integration over the cell volume.[58] Radial and angular points of the atomic grid were generated through Gauss−Legendre and Lebdev quadrature schemes. A grid pruning was adopted, as discussed in ref 58. In the present study, a (75, 974)p grid was used, such that it contains 75 radial points and a variable number of angular points, with a maximum of 974 on the Lebedev surface in the most accurate integration region. Full optimization (lattice constants and atomic positions) of CeO_2 and Ce_2O_3 were carried out using a convergence criterion of 3×10^{-4} hartree/bohr for the root-mean-square values of forces and 1.2×10^{-3} bohr in the root-mean-square values of atomic displacements. The Fermi level in the DOS plots is taken directly from CRYSTAL, and estimated in accordance with the zero-th level of the electrostatic energy in the multipolar Ewald-type expansion.[59]

3. Results and Discussion

3.1. Crystal Structure. By and large, DFT methods are known to predict fairly well the crystal structure of a wide variety of inorganic compounds. In general, the deviations of lattice parameters, both positive and negative, are in the range 2−3%,[60] hence it seems reasonable to adopt a value of 2.5% as accuracy criterion. Table 1 displays the computed lattice parameters for CeO_2 and Ce_2O_3 for each one of the functionals tested in this work. For comparison, some values chosen from the recent literature are also shown in this Table. In general, all computed values are found to correctly reproduce the experimental lattice parameters for both oxides, fulfilling the proposed accuracy criterion. The a_0 parameter for CeO_2 seems to be only modestly influenced by the exchange-correlation functional chosen. The largest errors correspond to the values computed with the B3LYP functional, the HH functional, or with the GGA+U approach (∼1.3%, 0.06−0.07 Å), although they are well below the required accuracy criterion. Alternatively, the smallest errors are found for the HHLYP, HSE and PBE0 functionals (less than 0.4%).

The a_0 and c_0 lattice parameters for Ce_2O_3 show a similar behavior: the computed values are quite insensitive to the functional chosen, with all calculated values within the proposed error bar. The HH functional is, again, the one with the largest errors with respect to the experimental values, underestimating by 1.5% and 1.9% the lattice parameters. It is worth pointing out that, except for the HSE functional,[23] the percent errors on the computed c_0 lattice parameter are larger than the errors found for the calculated a_0 values. As in the case of the lattice parameter of CeO_2, the smallest average errors are found for the HHLYP, HSE, and PBE0 functionals (less than 0.6% on average). Finally, it is worth mentioning here that the computed values with the PBE0 functional are practically the same, no matter the kind of basis set used: plane waves[23] or localized atomic orbitals (this work).

3.2. Electronic Structure. *3.2.1. Electronic Structure of CeO_2.* In CeO_2, the valence and conduction band are mainly composed by O 2*p* and Ce 5*d* states, respectively, while the Ce 4*f* states lie within the gap. All valence Ce states, including the 4*f* states, are empty, and the system is a wide gap insulator (see Figure 2, top). All local, semi local, and hybrid functionals produce an insulating solution, in agreement with the above picture of the CeO_2 electronic structure. Besides this qualitative agreement, the theoretical description of the electronic structure of CeO_2 is quite sensitive to the approach used, as can be deduced from the different band gaps reported in Table 2. As expected, both LDA and PBE underestimate the main band gap (O 2*p*− Ce 5*d*).[23] However, it is interesting to note that all DFT+U approaches reported in the literature also underestimate this band gap, and the results are not much sensitive to the specific value of the U parameter.[22,23] This can be easily explained since the U parameter acts only on the Ce 4*f* states, thus not modifying the relative positions of the valence and conduction bands, that have predominantly O 2*p* and Ce 5*d*

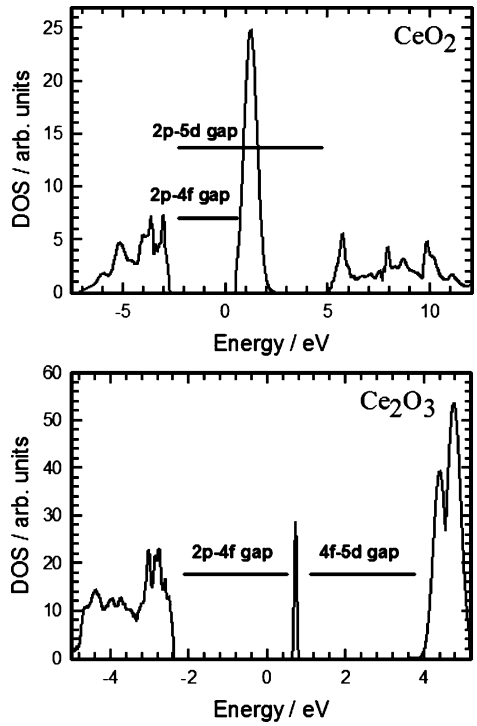

Figure 2. Total density of states (DOS) for CeO_2 (top) and Ce_2O_3 (bottom).

Table 2. Calculated and Experimental Band Gaps (in eV) for CeO_2

method	O 2*p*−Ce 5*d*	O 2*p*−Ce 4*f*	Ce 4*f* −Ce 5*d*
B3LYP	8.16	3.70	3.54
HH	10.64	7.50	1.91
HHLYP	10.75	7.18	2.51
PBE0	8.52	4.30	3.10
B1-WC	7.48	3.18	3.09
LDA[23]	5.61	2.0	2.25
PBE[23]	5.64	2.0	2.5
PBE0[23]	7.93	4.5	2.25
HSE[23]	6.96	3.5	2.25
HSE[28]	7.0	3.3	-
DFT+U[22,23]	∼ 5	-	-
Experiment[61,62,28]	∼ 6−8	2.6−3.9	

character. Alternatively, all hybrid functionals are found to produce larger values of the O 2*p* - Ce 5*d* gap. Particularly, the HH and HHLYP functionals result in an overly large error (∼3−4 *eV*) with respect to the experimental value[61] for this band gap. This behavior might be ascribed to an excessive weight (50%) of the exact exchange in these two functionals. Among the different hybrid possibilities tested in this work, the B1-WC functional is the one that produces the smallest O 2*p*−Ce 5*d* gap, 7.48 eV, in close agreement with XPS and BIS experimental data,[62] which indicate a conduction band about 3 eV wide centered at about 7.5 eV. The smaller gap found for B1-WC agrees with the fact that it is the one incorporating the lowest HF exchange fraction. However, it is worth noting that although the HF fraction in B1-WC is lower than that of the screened HSE hybrid, the latter gives a gap even smaller (∼7 eV), in excellent agreement with the experimental data.

Table 3. Calculated and Experimental Band Gaps (in eV) for Ce_2O_3

method	O 2*p*−Ce 5*d*	O 2*p*−Ce 4*f*	Ce 4*f* −Ce 5*d*
B3LYP	6.61	2.17	4.08
HH	9.4	1.83	7.19
HHLYP	9.78	1.13	8.25
PBE0	7.08	2.34	4.54
B1-WC	5.94	3.00	2.78
PBE0[23]	6.75	3.25	3.50
HSE[23]	5.75	3.25	2.50
experiment[18]			2.40

The results found for the O 2*p*−Ce 4*f* gap closely follow the behavior previously discussed for the main band gap. The HH and HHLYP functionals produce band gaps that are too large, mainly because the excessive weight of the exact exchange pushes upward all virtual levels. Among the remaining results, the B1-WC hybrid functional (with the lowest HF fraction) produces the lowest band gap, 3.18 eV, again in close agreement with available experimental data,[62] and with the HSE values (3.3−3.5 eV), which also fall in the experimental range. The use of the PBE0 approach results in a band gap slightly larger that the experimental data, a behavior already reported and discussed.[23]

3.2.2. Electronic Structure of Ce_2O_3. In contrast to CeO_2, in Ce_2O_3 one electron per Ce atom populates the Ce band, resulting in a narrow 4*f* occupied band that develops in the O 2*p*−Ce 5*d* gap, some 2.4 eV below the conduction band[18] that is formed mainly by a mixing of Ce 5*d* and Ce 4*f* states (see Figure 2, bottom). Overall, the effect of the inclusion of the exact exchange in the hybrid functionals is similar to those found in CeO_2. The HH and HHLYP functionals result in too large band gaps, with all virtual levels too high in energy. With respect to the remaining hybrid functionals used in this paper, again the B1-WC produces the best result for the Ce 4*f*−Ce 5*d* gap (2.78 eV). This value agrees reasonably with the experimental value available (2.40 eV) and is slightly higher that the one estimated using the HSE functional (2.50 eV), which actually is the best to reproduce the experiment. In any case, except for the aforementioned cases of the HH and HHLYP functionals, the computed electronic structure of Ce_2O_3 is in semiquantitative agreement with the experimental information. Finally, if we compare the PBE0 band gaps obtained either with plane-wave or GTO basis sets noticeable differences might be seen, indicating that the electronic structure is more implementation dependent than the lattice parameters.

3.3. Reaction Energies. Given the active and crucial role played by CeO_2 and Ce_2O_3 oxides in many heterogeneous chemical reactions, generally traced back to their oxygen storage capacity, we have also investigated the performance of different hybrid functionals on the computation of some reaction energies involving cerium oxides. The suitability to predict the relevant thermodynamic properties has been investigated by computing the energetics of two reduction reactions involving CeO_2 and Ce_2O_3, namely:

$$2CeO_2(s) \rightarrow Ce_2O_3(s) + 1/2O_2(g) \qquad (3)$$

$$2\,CeO_2(s) + CO(g) \rightarrow Ce_2O_3(s) + CO_2(g) \quad (4)$$

The reaction enthalpies have been calculated as

$$\Delta H_1 = E(Ce_2O_3) + 1/2\,E(O_2) - 2\,E(CeO_2) \quad (5)$$

$$\Delta H_2 = E(Ce_2O_3) + E(CO_2) - 2E(CeO_2) - E(CO) \quad (6)$$

where E(X) represents the computed total energies of X = CeO_2 (solid), Ce_2O_3 (solid), O_2(gas), CO_2 (gas), and CO (gas) per formula unit. The experimental values have been obtained from the corresponding heats of formation of reactants and products.[63] The computed reduction energies, along with the experimental values are reported in Table 4. Zero-point vibrational energy contributions have not been included. A major problem that we encounter which makes it hard to extract any conclusions with respect to the reliability of the different functionals is that the experimental heats of formation of cerium oxides are not easy to measure. This problem is related to difficulties in the preparation of defect-free oxides in a well-defined oxidation state. Comparing the most recent reported data for reaction 3, shown in Table 4, with other values available in the recent literature (3.57 eV),[2] the uncertainty in the experimental value might be estimated to be ~0.5 eV. With this caution in mind we can, anyhow, comment on the values computed in this work with different hybrid functionals. The estimated reaction energies for reaction 3 show a dispersion (standard deviation) of 0.67 eV, with an average value of 3.92 eV, in close agreement with the last reported experimental value. Excluding the HHLYP value, that shows the larger absolute error with respect the experimental value, the average reaction energy increases to 4.12 eV (slightly larger than the experiment) and the dispersion is reduced to 0.50 eV, similar to the experimental error bar. Thus, regarding the computed reaction energies for reaction 3 we can say that all theoretical values fit within the experimental error bar, being the HH and PBE0 functional the ones that produce the data with the smaller deviation with respect to the currently accepted experimental reaction enthalpy. However, we can see once again a significant difference between the PBE0 estimated values obtained using plane-waves or GTO as basis set.

In the case of reaction 4, we can assume a similar error bar for the experimental value reported. Similar comments can be made with respect to the computed theoretical values. Excluding again the value obtained with the HHLYP functional (that predicts an exothermic reaction), the calculated average reaction energy will be 0.80 eV, in close agreement with the experimental reaction enthalpy of 1.02 eV. The standard deviation of the theoretical values is, in this case, only 0.36 eV, well within the experimental error bar. In this case, the HH and B1-WC functionals produce the theoretical values in better agreement with the experimental data.

Table 4. Computed and Experimental Reaction Energies (in eV) for 2 $CeO_2 \rightarrow Ce_2O_3 + 1/2\ O_2$ and 2 CeO_2 + CO $\rightarrow Ce_2O_3 + CO_2$

	2 $CeO_2 \rightarrow Ce_2O_3 + 1/2\ O_2$		CeO_2 + CO $\rightarrow Ce_2O_3 + CO_2$	
method	ΔH	error	ΔH	error
B3LYP	3.52	−0.47	0.44	−0.58
HH	4.37	0.38	0.93	−0.09
HHLYP	2.88	−1.11	−0.16	−1.18
PBE0	3.66	−0.33	0.40	−0.62
B1-WC	4.45	0.46	1.05	0.03
PBE0[23]	3.14	−0.85		
HSE[23]	3.16	−0.83		
LDA+U[23]	3.04	−0.95		
PBE+U[23]	2.29	−1.70		
experiment[63]	3.99		1.02	

In summary, we can state that, excluding the HHLYP functional, all tested functionals produce values for the reaction energy that are within the experimental error bar of 0.5 eV.

3.4. Effect of the Fock Exchange. In addition, to evaluate the performance of different hybrid functionals in the description of the geometric and electronic structure of CeO_2 and Ce_2O_3, and in selected reaction energies involving ceria, we have also investigated to what extent the amount of HF exchange affects the three properties that we are looking at in this work: the cell parameters, the band gaps, and the reaction energies involved in the $Ce^{3+} \leftrightarrow Ce^{4+}$ redox process. Taking into account the results we have obtained so far, we have limited this analysis to the B3LYP, PBE0, and B1-WC functionals.

3.4.1. Cell Parameters. Figure 3 shows the influence of the amount of exact exchange in the computed values of the lattice parameters of CeO_2 and Ce_2O_3. Starting with the a_0 parameter of CeO_2, the computed lattice parameter decreases in all cases on increasing the percentage of HF exchange. This first result is in contrast with that reported on NiO, where the lattice constant was found to increase when the amount of exact exchange was raised.[40] For the PBE0 functional, the value computed with the standard amount of exact exchange (25%) is already very close to the experimental value, while for the B3LYP functional, the experimental lattice parameter is only reached at ~55% of exact exchange and for the B1-WC functional the most accurate value is obtained at 0% of exact exchange.

With respect to the lattice parameters of Ce_2O_3, we find that the a_0 parameter is quite insensitive to the amount of exact exchange in the three functionals tested. Only for the B3LYP functional, the experimental value of a_0 is reached (for 10−20% of HF exchange), while for PBE0 and B1-WC the computed value is always below the experimental one. The a_0 lattice parameter remains almost invariant with the B1-WC functional: the absolute change is less that 0.01 Å in the tested range (10−50% of HF exchange). The value of c_0 is more sensitive than that of a_0 to the fraction of HF exchange included in the hybrid functional. For the B3LYP and PBE0 functionals, the computed value decreases on increasing the participation of HF exchange, while for the B1-WC functional c_0 increases slightly. In the case of the PBE0 functional, the value closest to the experimental data is reached at about 10% of exact exchange, even though, with the standard value of HF exchange the error is only −0.35%, which is quite accurate and keeps the advantages of using a standard definition of the functional. In the case of the B3LYP functional, the experimental value of c_0 is

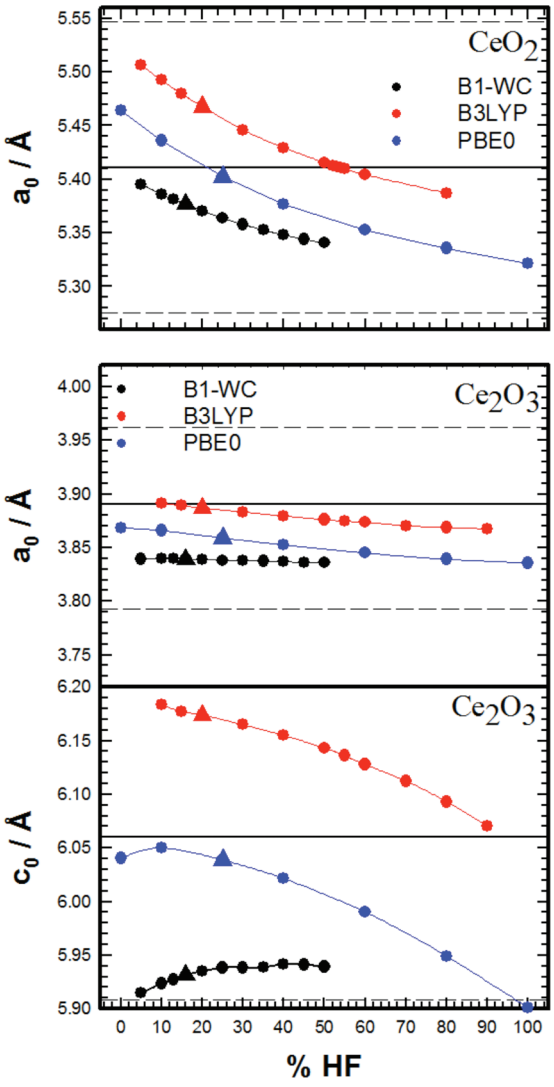

Figure 3. Dependency of the computed lattice parameters for CeO_2 (top) and Ce_2O_3 (a_0, middle and c_0, bottom) on the amount of exact exchange in the B3LYP, PBE0, and B1-WC functionals. The triangles denote the standard HF percent for each functional. The horizontal lines show the experimental value (full) and the acceptable error bars (dashed).

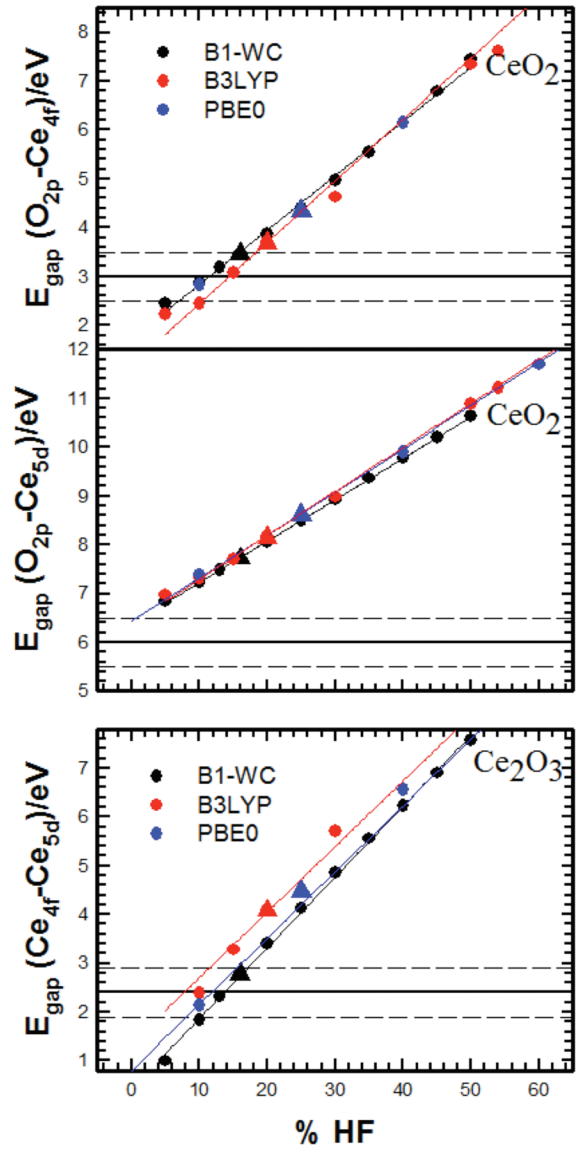

Figure 4. Dependency of the computed band gaps for CeO_2 (top and middle) and Ce_2O_3 (bottom) on the percentage of exact exchange in the B3LYP, PBE0, and B1-WC functionals. Refer to Figure 3 for labeling.

not reached for any amount of exact exchange, being only approximated when the amount of HF exchange if increased up to 90%. The variation of c_0 with the percentage of HF exchange in the B1-WC functional is (as it did happened with a_0) quite small. The computed lattice parameter increases only slightly in the tested range of exact exchange, the total increment being less than 0.05 Å.

In summary, the analysis of the variations in the cell structure suggests that overall the PBE0 at its original formulation is the more appropriate choice to simultaneously render the three parameters. Although in the case of the sesquioxide the B3LYP answer for a_0 is very good, it needs to incorporate a large amount of Fock exchange to get closer to the experimental c_0 value. In the general comparison the B1-WC functional seems to perform satisfactorily with small variations.

3.4.2. Band Gaps. The evolution of the computed band gaps with the amount of Fock exchange included in the functional shows, for the three functionals tested, a marked linear behavior (see Figure 4). In all cases, and in agreement with the well-known trend,[40,64] the computed band gaps increase with the amount of exact exchange, the increment being practically linear, showing similar slopes, with many of the fitting lines overlapping. A direct consequence of this behavior is that similar values of the band gaps are computed for similar contributions of the Fock exchange, regardless of the functional utilized. The O 2*p*−Ce 4*f* experimental band gap of CeO_2 is, thus, most approximated in the 10−15% range of exact exchange. On the contrary, the computed O 2*p*−Ce 5*d* band gap of CeO_2 is always larger than the experimental value of 6.0 eV,[61] but it approaches the ∼7.0−7.5 eV value[62] obtained from XPS and BIS data, for about 10% Fock exchange. In the case of Ce_2O_3, the experimental value is, again, more closely approached in the 10−15% range of exact exchange and the computed value increases linearly with increasing contribution of the HF exchange in the functional. It is particularly striking again

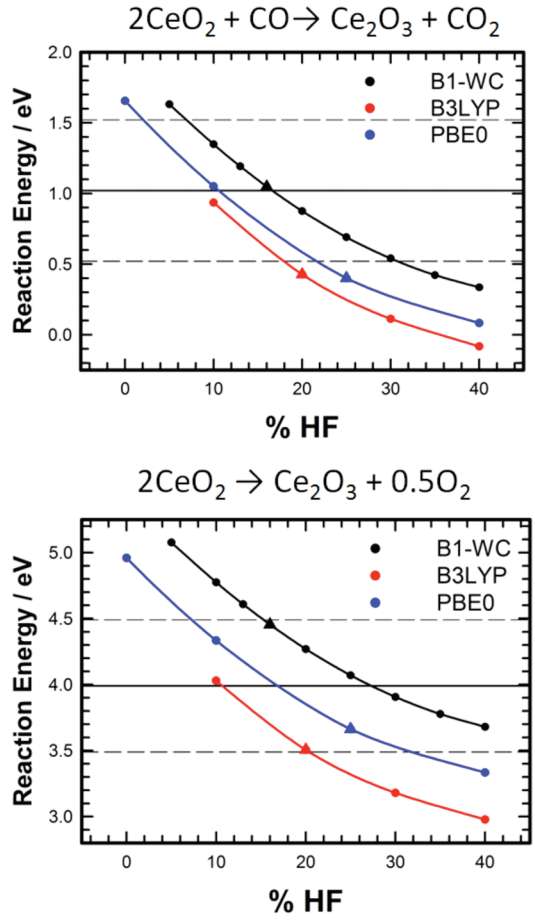

Figure 5. Dependency of the computed reaction energies on the percentage of exact exchange in the B3LYP, PBE0, and B1-WC functionals. Refer to Figure 3 for labeling.

that, regardless of the functional used, all experimental band gaps are nearly approximated in a similar range of HF exchange, around 10−15%. This can be interpreted in the sense that the different band gaps (the relative position of the bands) are mostly dependent on the exchange functional and basically independent of the correlation functional utilized.

Summarizing again, when we analyze the plots for the three band gaps reported in Figure 4, the B1-WC functional is the one that gives a better result. Only this functional at its original formulation is able to reproduce band gaps within the ±0.5 eV error bar, even though the O 2*p*−Ce 5*d* gap still is overestimated.

3.4.3. Energetics. The dependence on the computed reduction energies for reactions 3 and 4 on the percentage of HF exchange included in the functional is shown in Figure 5. In both cases, the estimated reaction energies are decreased on increasing the contribution of exact exchange and show a similar dependency as demonstrated by the curve fitted to the computed reaction energies. It is always possible to adjust the contribution of HF exchange to reproduce the experimental reaction energy. For the reduction of CeO_2 with CO, reaction 4, amounts of HF exchange of 10−15% seem to give the best agreement with the experimental reaction energy. For reaction 3, however, the dispersion of the computed reaction energy is larger and, as result, the percentage of HF exchange required to for the experimental value also spawns a larger range: ∼10% for B3LYP, ∼18% for PBE0, and ∼28% for the B1-WC functional. At its original formulation, the B1-WC functional is once again the best well-behaved functional as it is very accurate for reaction 4 and within the bar error in the case of reaction 3.

Table 5. Summary of the Effect of the Fock Exchange Contribution on the Structure, Band Gaps and Reaction Energies[a]

property	error limit	B3LYP(20)	PBE0(25)	B1WC(16)
structure (cell parameters)	2.5%	[0−100]	[0−100]	[0−100]
band-gaps CeO_2	0.5 eV	[10−18]	[8−16]	[8−16]
band-gaps Ce_2O_3	0.5 eV	[4−12]	[8−16]	[10−16]
energy for reaction 3	0.5 eV	[8−20]	[8−32]	[16−50]
energy for reaction 4	0.5 eV	[2−18]	[2−22]	[7−30]
the whole set		[10−12]	[8−16]	16

[a] Values that fulfill the accuracy criteria are in brackets, and the standard fractions between parentheses.

A complete view of the final ranges of possible HF fractions for which the different calculated values fall within the error bars might be obtained inspecting Table 5. As can be seen, the fraction for a given functional giving results within the error bars for lattice constants, band gaps, and energetics may differ, however, the three hybrids with the same nominal fraction of roughly 10−16% give results in fairly good agreement with the experimental data.

4. Conclusions

In this work, we report an analysis of the performance of five exchange-correlation functionals implemented in the CRYSTAL06 code to describe three properties of ceria that include crystal structure, band gaps, and reaction energies involved in the $Ce^{3+} \leftrightarrow Ce^{4+}$ redox process. Concerning the cell parameters, all five functionals give values that are within the 2.5% error, usually found for a vast majority of inorganic crystals, although the PBE0 hybrid functional is found to be the most accurate, giving parameters also very close to those estimated using the HSE screened functional. In general, when the fraction of HF exchange increases, a moderate lowering in the cell parameters is observed. Things change when we look at the band gaps of both cerium dioxide and sesquioxide. First the HH and HHLYP functionals lead to band gaps too large as they incorporate too much HF exchange that pushes the empty states too high. It is shown that for any functional used, the gaps are overestimated, and the agreement improves lowering the amount of the HF exchange. In this case, the overall best answer is provided by the B1-WC functional, which actually, among the functionals here considered, incorporates the lowest amount of HF exchange in its original formulation. The suitability to render the reaction energies normally involved in the rich ceria chemistry has been evaluated estimating the energetics associated to the $CeO_2 \rightarrow Ce_2O_3$ reduction process. For the two reactions considered, the reaction energies are in general underestimated, and lower when the amount of HF exchange increases, which is in contrast with the gaps behavior. Overall, the B1-WC functional is once again the most well-behaved functional to reproduce the correct energetics.

In summary, the present work shows that as far as the structure is concerned, any of the functionals that we have considered, in the original formulation, are accurate enough, giving parameters within the usual error bar. In general, the cell parameters are found to depend only moderately on the HF exchange fraction. However, caution should be taken in the case that the structure might favor a given state or property, in which case the PBE0 functional should be the choice. In the case of band gaps and reaction energies, a stronger dependency on the amount of HF exchange is observed. Its lowering improves band gaps and reaction energies with both PBE0 and B3LYP functional. Otherwise, at its standard formulation, the B1-WC functional (the one with the smallest fraction of HF exchange), seems to be the best choice as it provides good band gaps and reaction energies, and very reasonable crystal parameters.

Acknowledgment. This work has been supported by the Spanish Ministry of Science and Innovation, MICINN (Grant Nos. MAT2008-04918, CSD2008-0023), and the Junta de Andalucía (P08-FQM-3661). Computational time on the Barcelona Supercomputing Center/Centro Nacional de Supercomputación is gratefully acknowledged.

References

(1) Trovarelli, A. *Catal. Rev. Sci. Eng.* **1996**, *38*, 439.

(2) Trovarelli, A. *Catalysis by Ceria and Related Materials; Catalytic Science Series*; Imperial College Press: London, 2002; Vol. 2.

(3) Dictor, R.; Roberts, S. *J. Phys. Chem.* **1989**, *93*, 5846.

(4) Su, E. C.; Rothschild, W. G. *J. Catal.* **1986**, *99*, 506.

(5) Yao, H. C.; Yu Yao, Y. F. *J. Catal.* **1984**, *86*, 254.

(6) Engler, B.; Koberstein, E.; Schubert, P. *Appl. Catal.* **1989**, *48*, 71.

(7) Miki, T.; Ogawa, T.; Haneda, M.; Kakuta, N.; Ueno, A.; Tateishi, S.; Matsuura, S.; Sato, M. *J. Phys. Chem.* **1990**, *94*, 6464.

(8) Daniell, W.; Ponchel, A.; Kuba, S.; Anderle, F.; Weingand, T.; Gregory, D. H.; Knozinger, H. *Top. Catal.* **2002**, *20* (1−4), 65–74.

(9) Wachs, I. E. *Catal. Today* **2005**, *100*, 79–94.

(10) Dinse, A.; Frank, B.; Hess, C.; Habel, D.; Schomacker, R. *J. Mol. Catal. A* **2008**, *289*, 28–37.

(11) Ganduglia-Pirovano, M. V.; Popa, C.; Sauer, J.; Abbott, H.; Uhl, A.; Baron, M.; Stacchiola, D.; Bondarchuk, O.; Shaikhutdinov, S.; Freund, H.-J. *J. Am. Chem. Soc.* **2010**, *132*, 2345.

(12) Shido, T.; Iwasawa, Y. *J. Catal.* **1992**, *136*, 493.

(13) Shido, T.; Iwasawa, Y. *J. Catal.* **1993**, *141*, 71.

(14) Park, J. B.; Graciani, J.; Evans, J.; Stacchiola, D.; Ma, S. G.; Liu, P.; Nambu, A.; Sanz, J. F.; Hrbek, J.; Rodriguez, J. A. *Proc. Natl. Acad. Sci.* **2009**, *106*, 4975.

(15) Rodriguez, J. A.; Graciani, J.; Evans, J.; Park, J. B.; Yang, F.; Stacchiola, D.; Senanayake, S. D.; Ma, S.; Perez, M.; Liu, P.; Sanz, J. F.; Hrbek, J. *Angew. Chem., Int. Ed.* **2009**, *48*, 8047.

(16) Park, J. B.; Graciani, J.; Evans, J.; Stacchiola, D.; Senanayake, S. D.; Barrio, L.; Liu, P.; Sanz, J. F.; Hrbek, J.; Rodriguez, J. *J. Am. Chem. Soc.* **2010**, *132*, 356.

(17) Trovarelli, A.; de Leitenburg, C.; Boaro, M.; Dolcetti, G. *Catal. Today* **1999**, *50*, 353.

(18) Prokofiev, A.; Shelykh, A.; Melekh, B. *J. Alloys Compd.* **1996**, *242*, 41.

(19) Yang, Z.; Woo, T. K.; Baudin, M.; Hermansson, K. *J. Chem. Phys.* **2004**, *120*, 7741.

(20) Nolan, M.; Grigoleit, S.; Sayle, D. C.; Parker, S. C.; Watson, G. W. *Surf. Sci.* **2005**, *576*, 217.

(21) Andersson, D. A.; Simak, S. I.; Johansson, B.; Abrikosov, I. A.; Skorodumova, N. V. *Phys. Rev. B* **2007**, *75*, 035109.

(22) Loschen, C.; Carrasco, J.; Neyman, K.; Illas, F. *Phys. Rev. B* **2007**, *75*, 035115.

(23) Da Silva, J. L. F.; Ganduglia-Pirovano, M. V.; Sauer, J.; Bayer, V.; Kresse, G. *Phys. Rev. B.* **2007**, *75*, 045121.

(24) Da Silva, J. L. F. *Phys. Rev. B* **2007**, *76*, 193108.

(25) Castleton, C. W. M.; Kullgren, J.; Hermansson, K. *J. Chem. Phys.* **2007**, *127*, 244704.

(26) Kresse, G.; Blaha, P.; Da Silva, J. L. F.; Ganduglia-Pirovano, M. V. *Phys. Rev. B* **2005**, *72*, 237101.

(27) Heyd, J.; Scuseria, G. E. *J. Chem. Phys.* **2006**, *125*, 224106.

(28) Hay, P. J.; Martin, R. L.; Uddin, J.; Scuseria, G. E. *J. Chem. Phys.* **2006**, *125*, 034712.

(29) Ganduglia-Pirovano, M. V.; Da Silva, J. L. F.; Sauer, J. *Phys. Rev. Lett.* **2009**, *102*, 026101.

(30) Fabris, S.; de Gironcoli, S.; Baroni, S.; Vicario, G.; Balducci, G. *Phys. Rev. B* **2005**, *72*, 237102.

(31) Cococcioni, M.; de Gironcoli, S. *Phys. Rev. B* **2005**, *71*, 035105.

(32) Jiang, H.; Gomez-Abal, R. I.; Rinke, P.; Scheffler, M. *Phys. Rev. Lett.* **2009**, *102*, 126403.

(33) Duclos, S. J.; Vohra, Y. K.; Ruoff, A. L.; Jayaraman, A.; Espinosa, G. P. *Phys. Rev. B* **1988**, *38*, 7755.

(34) Gerward, L.; Olsen, J. S. *Powder Diffr.* **1993**, *8*, 127.

(35) Branda, M. M.; Hernández, N. C.; Sanz, J. F.; Illas, F. *J. Phys. Chem. C* **2010**, *114*, 1934.

(36) Hernández, N. C.; Grau-Crespo, R.; de Leeuw, N. H.; Sanz, J. F. *Phys. Chem. Chem. Phys.* **2009**, *11*, 5246.

(37) Branda, M. M.; Castellani, N. J.; Grau-Crespo, R.; de Leeuw, N. H.; Cruz Hernandez, N.; Sanz, J. F.; Neyman, K. M.; Illas, F. *J. Chem. Phys.* **2009**, *131*, 94702.

(38) Kullgren, J.; Castleton, Ch. W. M.; Müller, C.; Muñoz-Ramo, D.; Hermansson, K. *J. Chem. Phys.* **2010**, *132*, 054110.

(39) Martin, R. L.; Illas, F. *Phys. Rev. Lett.* **1997**, *79*, 1539.

(40) Moreira, I. de P. R.; Illas, F.; Martin, R. L. *Phys. Rev. B* **2002**, *65*, 155102.

(41) Dovesi, R.; Saunders, V. R.; Roetti, C.; Orlando, R.; Zicovich-Wilson, C. M.; Pascale, F.; Civarelli, B.; Doll, K.; Harrison, N. M.; Bush, I. J.; D'Arco, P.; Llunell, M. *CRYSTAL06 User's Manual*; Universita di Torino: Torino, 2006.

(42) Parr, R. G.; Yang, W. *Density Functional Theory of Atoms and Molecules*; Oxford University Press: New York, 1989.

(43) Adamo, C.; Barone, V. *Chem. Phys. Lett.* **1998**, *298*, 113.

(44) Becke, A. D. *J. Chem. Phys.* **1993**, *98*, 1372.

(45) Becke, A. D. *J. Chem. Phys.* **1993**, *98*, 5648.

(46) Lee, C.; Yang, W.; Parr, R. G. *Phys. Rev. B* **1998**, *37*, 785.

(47) Miehlich, B.; Savin, A.; Stoll, H.; Preuss, H. *Chem. Phys. Lett.* **1989**, *157*, 200.

(48) Bilc, D. I.; Orlando, R.; Rignanese, G. M.; Íñiguez, J.; Ghosez, P. *Phys. Rev. B* **2008**, *77*, 165107.

(49) Perdew, J. P.; Burke, K.; Ernzerhof, M. *Phys. Rev. Lett.* **1996**, *77*, 3865.

(50) Dirac, P. A. M. *Proc. Cambridge Phil. Soc.* **1930**, *26*, 376.

(51) Vosko, S. H.; Wilk, L.; Nusair, M. *Can. J. Phys.* **1980**, *58*, 1200.

(52) Becke, A. D. *Phys. Rev. A* **1988**, *38*, 3098.

(53) Wu, Z.; Cohen, R. E. *Phys. Rev. B* **2006**, *73*, 235116.

(54) Dolg, M.; Stoll, H.; Preuss, H. *J. Chem. Phys.* **1989**, *90*, 1730.

(55) The CRYSTAL web page: http://www.crystal.unito.it

(56) Corà, F. *Mol. Phys.* **2005**, *103*, 2483.

(57) Monkhorst, H. J.; Pack, J. D. *Phys. Rev. B* **1976**, *13*, 5188.

(58) Pascale, F.; Zicovich-Wilson, C. M.; López Gejo, F.; Civarelli, B.; Orlando, R.; Dovesi, R. *J. Comput. Chem.* **2004**, *25*, 888.

(59) Saunders, V. R.; Freyria-Fava, C.; Dovesi, R.; Salasco, L.; Roetti, C. *Mol. Phys.* **1992**, *77*, 629.

(60) Sholl, D. S.; Steckel, J. A. In *Density Functional Theory: A Practical Introduction*; John Wiley and Sons: Hoboken, NJ, 2009, p 222.

(61) Marabelli, F.; Wachter, P. *Phys. Rev. B* **1987**, *36*, 1238.

(62) Wuilloud, E.; Delley, B.; Schneider, W. D.; Baer, Y. *Phys. Rev. Lett.* **1984**, *53*, 202.

(63) Lide, D. R., Ed. *CRC Handbook of Chemistry and Physics*, 9th ed.; CRC Press, Boca Raton, Florida, U.S.A., 2009).

(64) Muscat, J.; Wander, A.; Harrison, N. M. *Chem. Phys. Lett.* **2001**, *342*, 397.

CT100430Q